

*Supplementary Information for*

**Hydrogen bond-mediated strong adsorbent-I<sub>3</sub><sup>-</sup> interactions  
enable high-efficiency radioiodine capture**

Juan Wang<sup>ab</sup>, Zelun Li<sup>a</sup>, Ying Wang<sup>a</sup>, Changting Wei<sup>a</sup>, Kelong Ai<sup>\*ab</sup> and Lehui Lu<sup>\*ab</sup>

<sup>a</sup> State Key Laboratory of Electroanalytical Chemistry, Changchun Institute of Applied Chemistry, Chinese Academy of Sciences, Changchun, Jilin, 130022, China.

<sup>b</sup> University of Science and Technology of China, Hefei, Anhui, 230026, China.

**\*Corresponding Author**

E-mail: [klai@ciac.ac.cn](mailto:klai@ciac.ac.cn); [lehuilu@ciac.ac.cn](mailto:lehuilu@ciac.ac.cn).

## Materials and Instrumentations:

Paraformaldehyde, cesium triiodide, MOR, ZSM, copper (I) iodide were bought from Sigma-Aldrich. Methyl iodide (99%) and ethyl iodide (99%) were purchased from Aladdin Reagents Co. Ltd. (Shanghai, China). All other reagents and solvents were obtained from commercial suppliers in reagent grade purity or higher and were used without further purification. TEM images were taken by a TECNAI G2 high-resolution transmission electron microscope. The SEM images were collected on an FEI/Philips XL30 ESEM FEG field-emission scanning electron microscopy system. HRTEM and HAADF-STEM images were performed on a Hitachi H-8100 TEM system. The XPS spectra were recorded on a VG ESCALAB MKII X-ray photoelectron spectrometer. FTIR spectra were obtained on a Bruker Vertex 70 spectrometer. Thermo gravimetric analyze (TGA) were conducted by using a Perkin-Elmer TGA-2 thermo gravimetric analyzer in N<sub>2</sub> from room temperature to 600 °C at a rate of 10 °C min<sup>-1</sup>. The XRD patterns were measured on a D8 ADVANCE (Germany) using Cu-K $\alpha$  (0.15406 nm) radiation. The Raman spectrum was obtained using a Renishaw Raman system model 2000 spectrometer. Nitrogen adsorption and desorption isotherms were measured at 77 K with a Quadrachrome adsorption instrument. Pore size distributions (PSD) were calculated using the adsorption branch of the isotherms by the DFT method. UV-Vis absorption analysis was performed with a Cary 50 scan UV-Vis-NIR spectrophotometer (Varian). Elemental analysis was conducted on a Vario EL cube (Elementar Analysensysteme GmbH) to determine carbon, nitrogen, hydrogen, and sulfur contents in the samples. <sup>1</sup>H NMR spectra were recorded on Bruker MSL-300 spectrometers. The chemical shift scales were referenced to TMS. N<sub>2</sub>, O<sub>2</sub> and NO<sub>2</sub> were analyzed by a GC (Kechuang, GC 9800) equipped with a TCD, using a packed TDX-01 (1 m) and molecular sieve 5A column (1.5 m). The XAS experiments (XANES and EXAFS experiments) were performed at the BL14W139 station in Shanghai Synchrotron Radiation Facility (SSRF). All the spectra were collected at room temperature in transmission mode. The I K-edges data were collected using a fixed-exit double-crystal Si (311) monochromator. The raw data analysis was performed using IFEFFIT software package according to the standard data analysis procedures. Data fitting was done by Artemis program in IFEFFIT.

## Synthesis of benchmark materials:

**Preparation of Si-BEA crystals.** Si-BEA was prepared from a gel consisting of fumed silica, TEAOH, (NH<sub>4</sub>)<sub>2</sub>SiF<sub>6</sub>, KOH and H<sub>2</sub>O by adopting the literature procedure <sup>1</sup>. The molar ratio of the components in the gel was 4.00: 1.92: 0.36: 0.40: 31.20. The hydrothermal reaction was carried out at 165 °C. After 7 days of reaction, the autoclave was removed from the oven and quickly cooled to room temperature by running tap water onto them. The obtained crystals were thoroughly washed with copious amounts of distilled deionized water and dried at 100 °C by placing them in an oven overnight.

**Synthesis of Ag<sup>+</sup>@MOR.** Ag<sup>+</sup>@ MOR was synthesized according to the previously reported procedure <sup>2</sup>. Typically, 1 g MOR was added into a 100 ml AgNO<sub>3</sub> solution (1 M), and the mixture was stirred for 24 h and the samples were obtained by filtrate and wash with H<sub>2</sub>O. Such exchange procedure was repeated twice to obtain the final samples.

**Synthesis of Ag<sup>0</sup>@MOR.** Ag<sup>0</sup>@MOR was synthesized by hydrogenation of Ag<sup>+</sup>@MOR under H<sub>2</sub> environment at 200 °C for 12 h.

**Synthesis of Ag<sup>+</sup>@ZSM-5.** The same synthetic procedure as for Ag<sup>+</sup>@MOR was used except that MOR was replaced by ZSM-5.

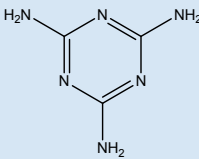
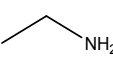
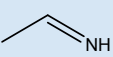
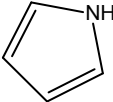
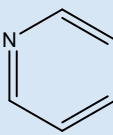
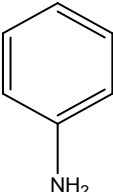
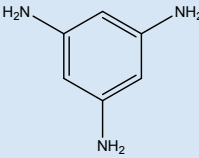
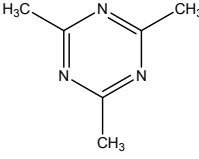
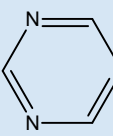
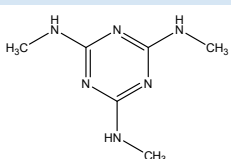
**Synthesis of ZIF-8<sup>3</sup>.** Methanolic solutions of zinc nitrate (25 mM, 15 ml) and 2-methylimidazole (25 mM, 15 ml) were mixed and allowed to react at room temperature for 24 h without stirring. The product was collected by centrifugation, washed several times with methanol, and vacuum-dried overnight at room temperature.

**Synthesis of CMP.** The CMP was synthesized according to the literature <sup>4</sup>. 3,3',5,5'-tetrabromo-2,2'-bithiophene (481.8 mg, 1 mmol) and 1,4-diethynylbenzene (189.2 mg, 1.5 mmol), tetrakis (triphenylphosphine) palladium (0) (90 mg), and copper (I) iodide (30 mg) were mixed and filled with nitrogen for 20 min. After that, a mixture of toluene (5 mL) and triethylamine (5 mL) were added. Then the mixture was heated to 65 °C and stirred for 24 h under nitrogen atmosphere. The mixture was filtered and washed with methylene dichloride, acetone, water and methanol for several times. Finally, the polymer was further purification by Soxhlet extraction (methanol) for 72 h.

## **NO<sub>2</sub> breakthrough experiments**

The NO<sub>2</sub> adsorption experiments were measured by using a mass spectrometer (QIC-20, Hiden). In a typical experiment, 100 mg of the sample was loaded into a quartz tube (Φ8mm) and supported using quartz wool. Before the test, sample was pretreated with Ar and flushed for 3 h to reach a stable background and then flow Ar 20 ml/min, mixtures gas 5-10 ml/min.

**Table S1.** The comparisons of a series of molecules that possible bind with  $I_3^-$ .

Number	Chemical Name	Structural Formula	Binding Energy (kcal/mol)	Main Binding Sites
1	melamine		-37.41	N—H • • • I N—H • • • I
2	ethylamine		-20.16	N—H • • • I
3	ethanimine		-20.87	C—H • • • I N—H • • • I
4	pyrrole		-24.36	N—H • • • I
5	pyridine		-21.66	C—H • • • I
6	aniline		-22.47	N—H • • • I N—H • • • I
7	1,3,5-benzenetriamine		-20.89	N—H • • • I
8	trimethyl-triazine		-31.85	C—H • • • I
9	1,3,5-triazine		-18.68	C—H • • • I
10	trimethyl-melamine		-30.50	N—H • • • I N—H • • • I

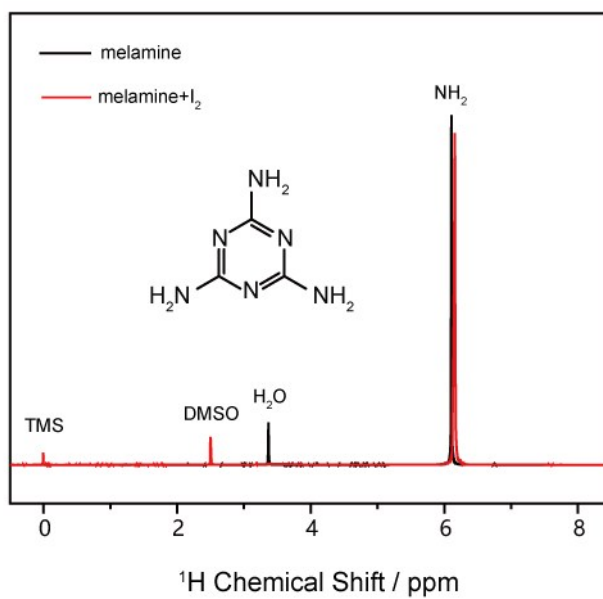
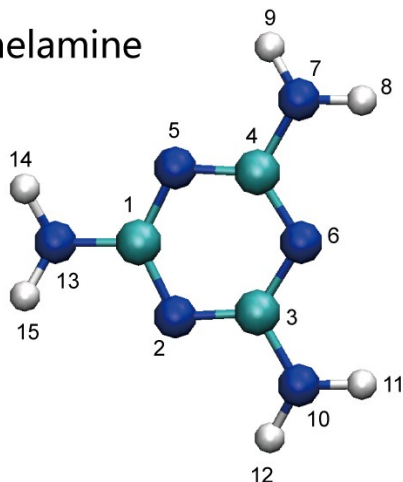


**Figure S1.**  $^1\text{H}$  NMR of melamine molecules before and after loading iodine. The amines of melamine shifted downfield in the  $\text{I}_2$ -laden state, while other peaks were invariant. This result implied that the H atoms were responsible for binding with iodine.

melamine

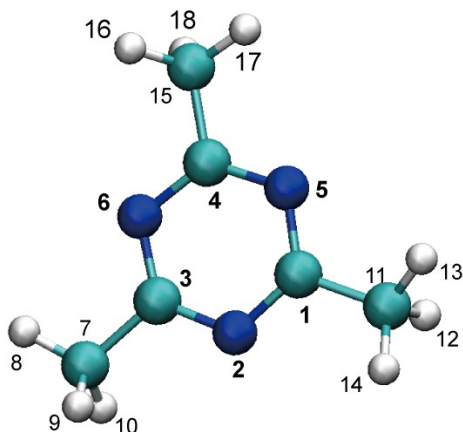


Mulliken charges:

1			
1 C	0.2804	2 N	-0.3436
3 C	0.2804	4 C	0.2804
5 N	-0.3436	6 N	-0.3436
7 N	-0.4034	8 H	0.2333
9 H	0.2333	10 N	-0.4034
11 H	0.2333	12 H	0.2333
13 N	-0.4034	14 H	0.2333
15 H	0.2333		

Sum of Mulliken charges = -0.0000

trimethyl-triazine



Mulliken charges:

1			
1 C	0.2083	2 N	-0.2481
3 C	0.2083	4 C	0.2083
5 N	-0.2481	6 N	-0.2481
7 C	-0.3312	8 H	0.1236
9 H	0.1236	10 H	0.1236
11 C	-0.3312	12 H	0.1236
13 H	0.1236	14 H	0.1236
15 C	-0.3312	16 H	0.1236
17 H	0.1236	18 H	0.1236

Sum of Mulliken charges = -0.0000

**Figure S2.** The Mulliken charges distribution of each atom in melamine and trimethyl-triazine molecule. The triazine ring has strong electron-withdrawing ability, which could decrease the electron density of H atom in melamine and trimethyl-triazine and promote its binding with  $I_3^-$ .

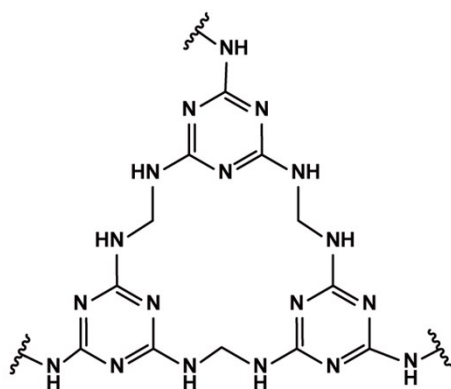


**Figure S3.** Chemical structure of the MFP network.

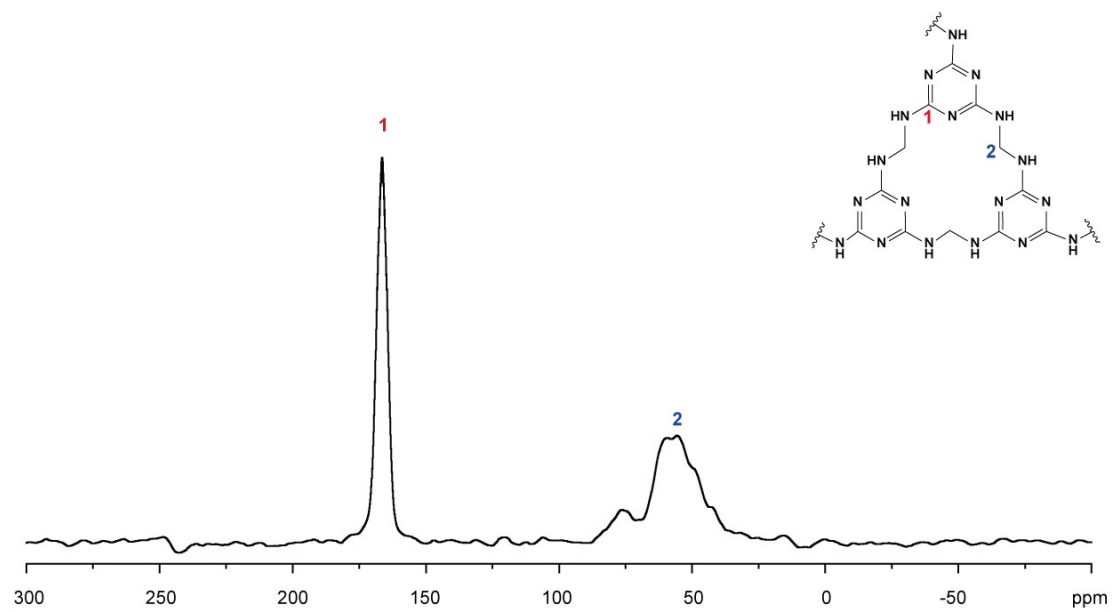


**Figure S4.**  $^{13}\text{C}$  solid-state nuclear magnetic resonance (SSNMR) spectra of MFP.

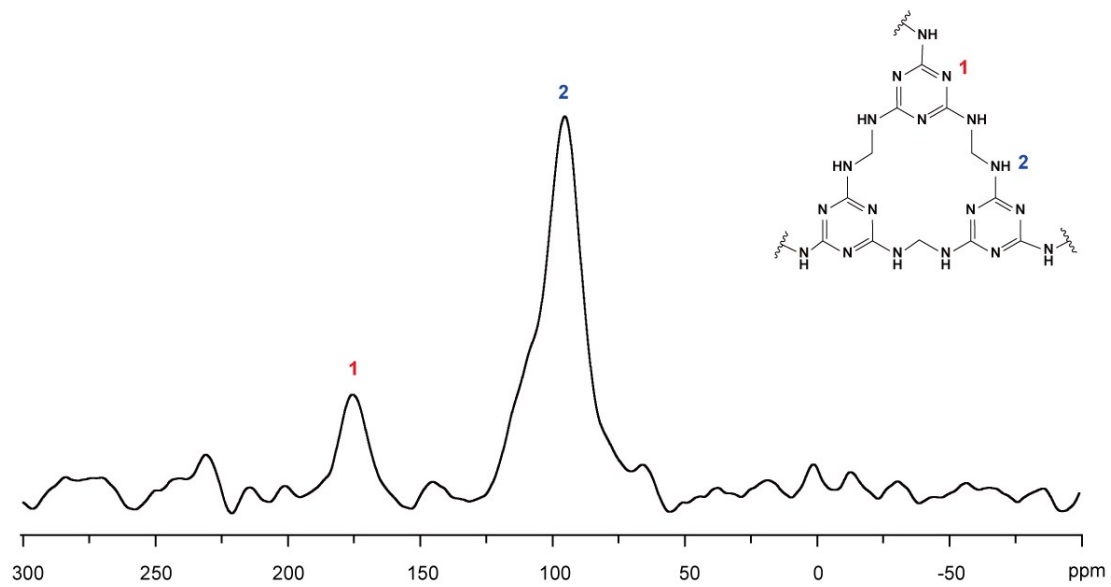


**Figure S5.**  $^{15}\text{N}$  solid-state nuclear magnetic resonance (SSNMR) spectra of MFP.

**Table S2.** Pore properties of MFP materials.

$S_{\text{BET}} / \text{m}^2 \text{g}^{-1}$	$\text{PV}^{[\text{a}]} / \text{cc g}^{-1}$	$\text{PV}^{[\text{b}]} / \text{cc g}^{-1}$	$\text{MPV}^{[\text{c}]} / \text{cc g}^{-1}$
1440	2.677	2.513	0.544

[a] Pore volume calculated from nitrogen adsorption at  $p/p_0=0.99$ . [b] Pore volume calculated from DFT method. [c] Micropore volume calculated from HK method. MFP polymers could achieve high surface areas of up to  $1440 \text{ m}^2 \text{g}^{-1}$ , total pore volumes  $2.677 \text{ cc/g}$ , and micropore volumes  $0.544 \text{ cc/g}$ .

**Table S3.** Elemental analysis showed that the different composition content of MFPS synthesized under different proportion of raw materials.

Entry	Molar ratio <sup>[a]</sup>	N /[%]	C /[%]	H /[%]	S /[%]	O /[%]	S <sub>BET</sub> / m <sup>2</sup> g <sup>-1</sup>	Capacity / mg/g
1	1/1.5	45.45	38.99	4.59	6.34	4.63	832	5505
2	1/3	45.22	39.08	5.05	5.68	4.97	1060	5911
3	1/3.5	44.9	39.18	5.18	5.76	4.98	944	5856
4	1/4	44.05	39.74	5.2	6.35	4.66	1135	6010
5	1/4.5	43.76	39.94	5.17	6.38	4.75	1440	6370
6	1/5	41.72	40.33	5.34	6.88	5.73	925	5639
7	1/6	40.47	41.66	5.59	7.74	4.54	1213	5825

[a] Molar ratio of melamine to paraformaldehyde. In this experiment, the amount of melamine was the same, and the amount of paraformaldehyde was gradually increased. With the increasing amount of paraformaldehyde, the N content in elemental analysis decrease, and the C content increase, indicating that the degree of polymerization of materials is higher and higher. The elemental analysis and S<sub>BET</sub> results indicated that the high surface area and moderate degree of polymerization are conducive to maximizing the adsorption capacity.

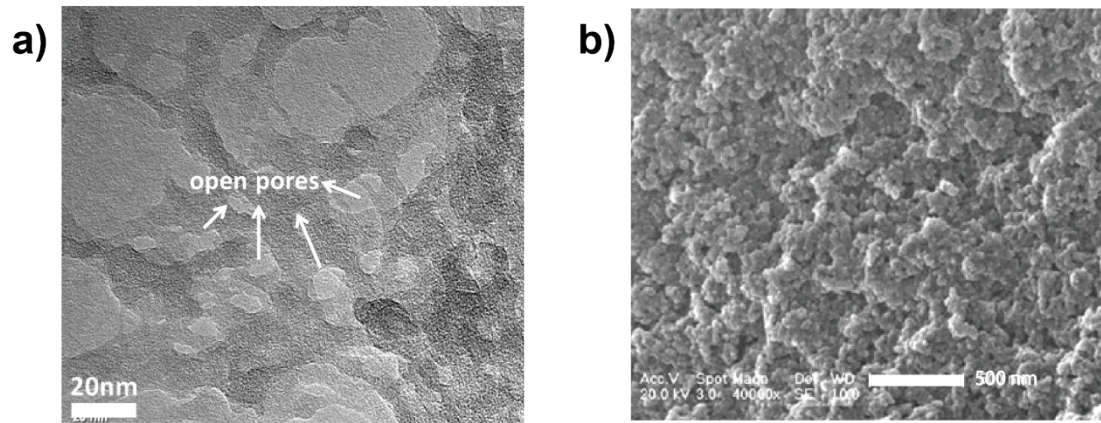


**Figure S6.** The HRTEM image (a) and SEM image (b) of the pristine MFP.

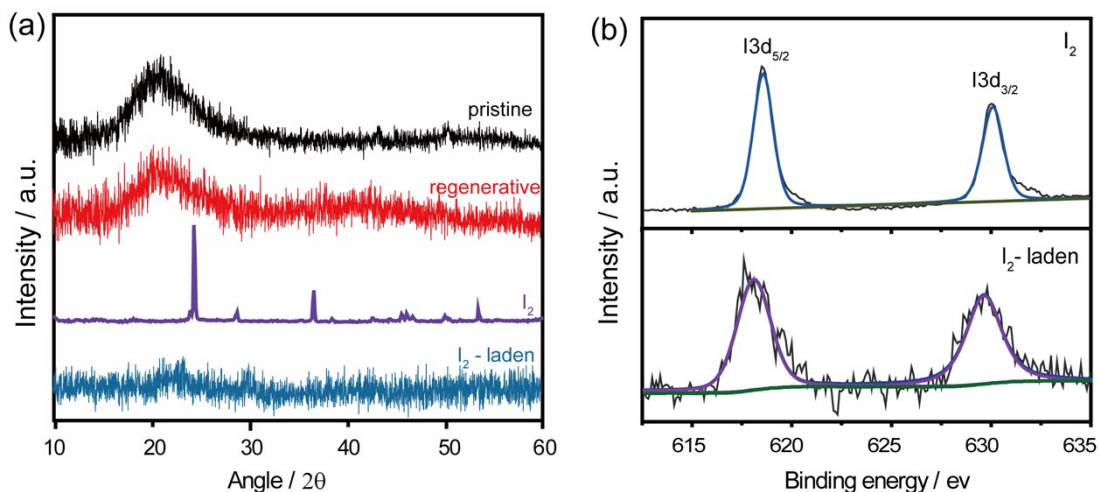


**Figure S7.** (a) XRD patterns of pristine MFP, I<sub>2</sub>, I<sub>2</sub>-laden MFP, and regenerative MFP after ethanolamine washing. MFP shows one broad diffraction peak centered at  $2\theta = 21^\circ$ , which was assigned to the amorphous carbon. After loading iodine, the I<sub>2</sub>-laden MFP did not display the signal peak of iodine, resulting from I<sub>2</sub> have converted into I<sub>3</sub><sup>-</sup> species. And the broad diffraction peak of MFP dropped significantly as the large amount of iodine doping. Then the characteristic peak recovered after washed with ethanolamine, suggesting MFP could be reused. (b) XPS spectra of I<sub>2</sub> and I<sub>2</sub>-laden MFP. The binding energy of I3d<sub>5/2</sub> and I3d<sub>3/2</sub> belongs to I<sub>2</sub> located at 618.6eV and 630.1eV, respectively. After iodine loading, the binding energy of MFP sample shifted to 618.1eV and 629.6eV, which can be attributed to I<sub>3</sub><sup>-</sup>.

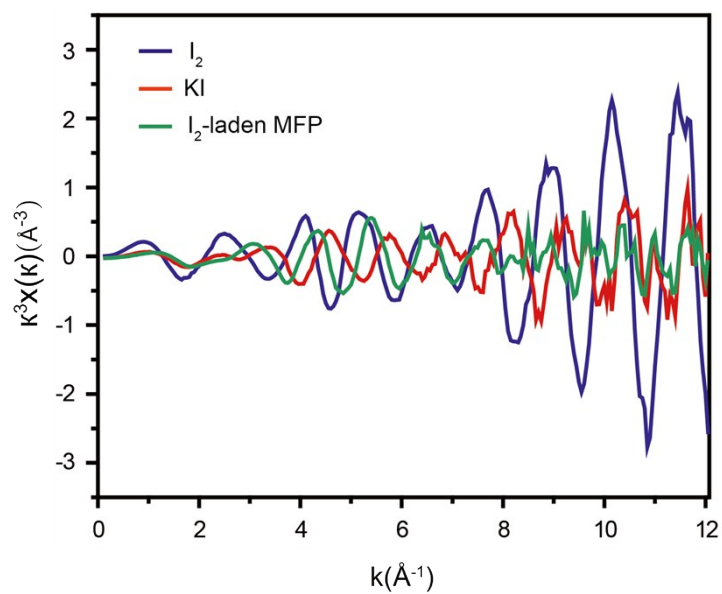


**Figure S8.** The  $k^3$ -weighted I K-edge EXAFS spectrum for  $I_2$ -laden MFP.  $I_2$  and KI were used as references.

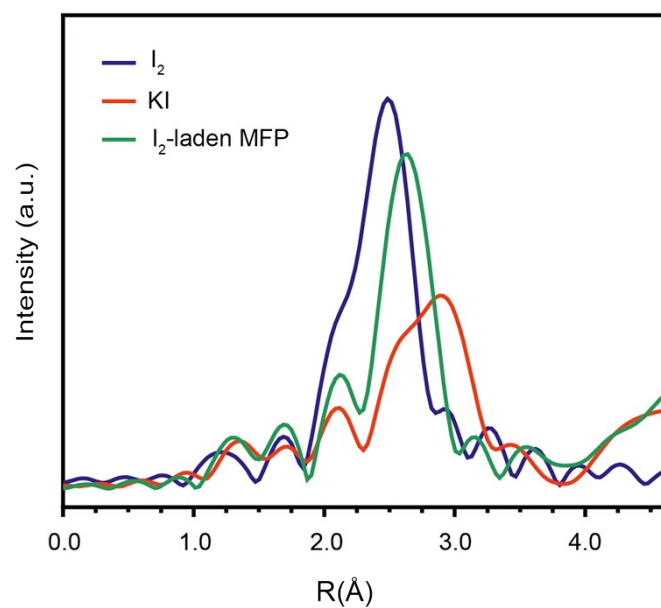


**Figure S9.** The  $k^3$ -weighted Fourier transform spectrum from I K-edge EXAFS data for  $I_2$ -laden MFP.  $I_2$  and KI were used as the references.

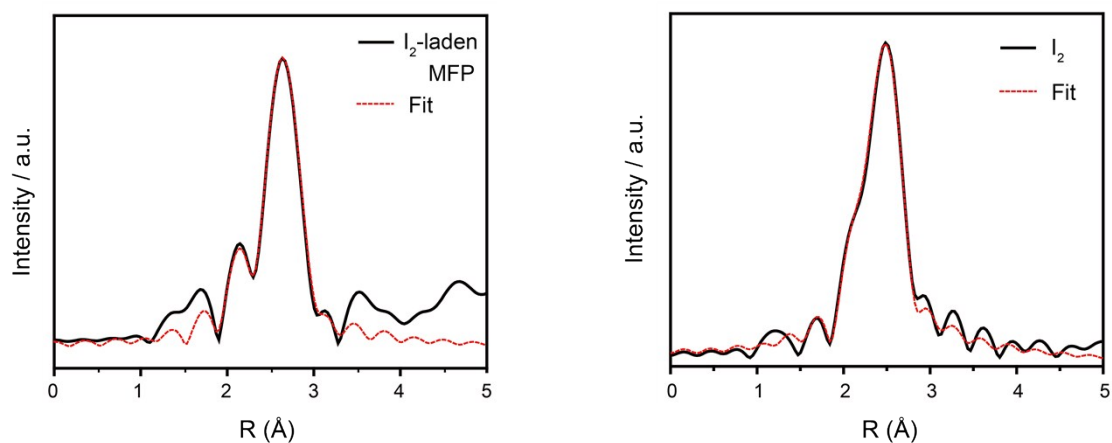


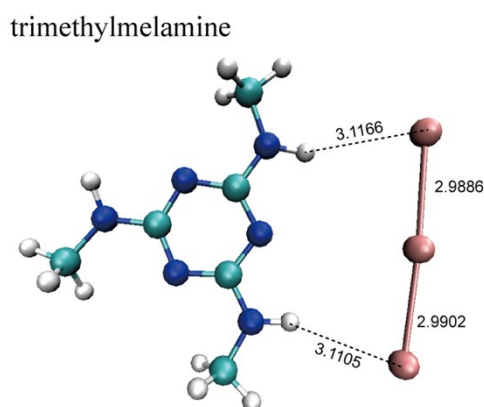
**Figure S10.** The Fourier-transformed I K-edge EXAFS spectra and the corresponding fitting curves for I<sub>2</sub>-laden MFP and I<sub>2</sub>. The corresponding curve fit results are presented in Table S3. The dashed lines are the corresponding fitted curves.

**Table S4.** Fitting parameters for I K-edge EXAFS spectra of I<sub>2</sub>-laden MFP.

<i>Sample</i>	<i>R(Å)</i>	<i>CN</i>	<i>σ<sup>2</sup></i>
I <sub>2</sub> -laden MFP	2.92	1.1	0.0082
I <sub>2</sub>	2.72	1.0	0.0024

R (Å): bond length, CN: coordination number,  $\sigma^2$  (Å<sup>2</sup>): Debye-Waller factor. I<sub>2</sub> was used as reference.

(a)



(b)

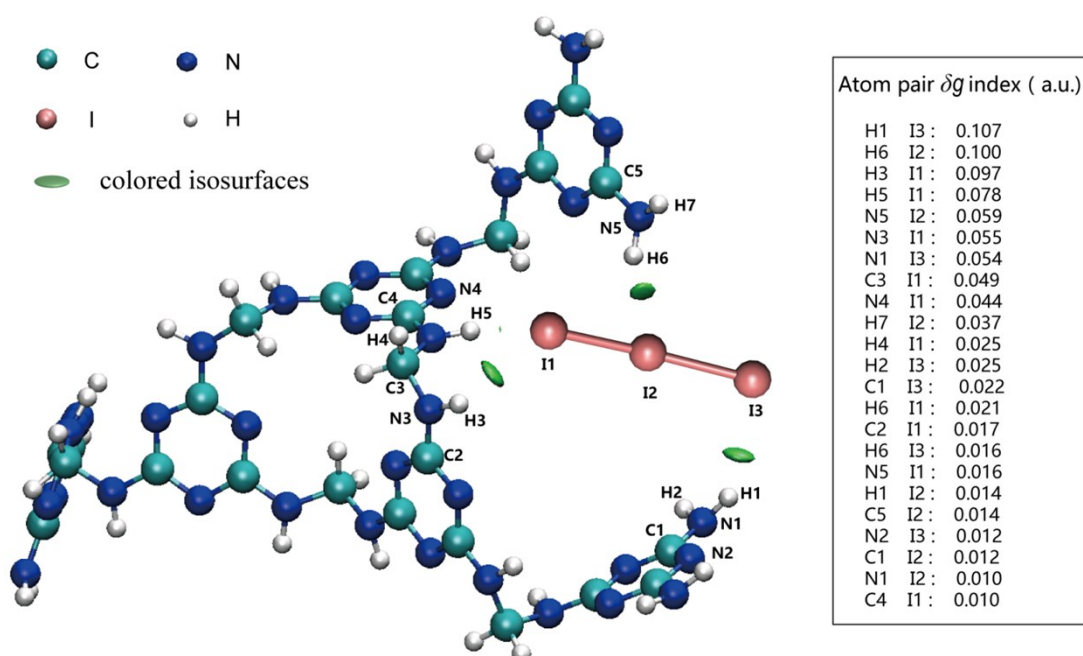


**Figure S11.** (a) Trimethyl-melamine bound with  $I_3^-$ ; the binding energy was calculated to be -30.5 Kcal/mol. (b) The calculated atom pair index of MFP and  $I_3^-$ . The N-H...I hydrogen bond plays a leading role in interacting MFP with  $I_3^-$ , and N...I and C...I halogen bonds also assist this interaction (Smaller values are not showed). The bond angle of  $I_3^-$  species and amino groups are as follows:  $\angle I_2-I_3-H_1:97.10^\circ$ ,  $\angle I_2-I_3-H_2:90.61^\circ$ ,  $\angle I_2-I_1-H_3:114.14^\circ$ ,  $\angle I_2-I_1-H_5:98.33^\circ$ ,  $\angle I_1-I_2-H_6:86.77^\circ$ ,  $\angle I_1-I_2-H_7:84.22^\circ$ .

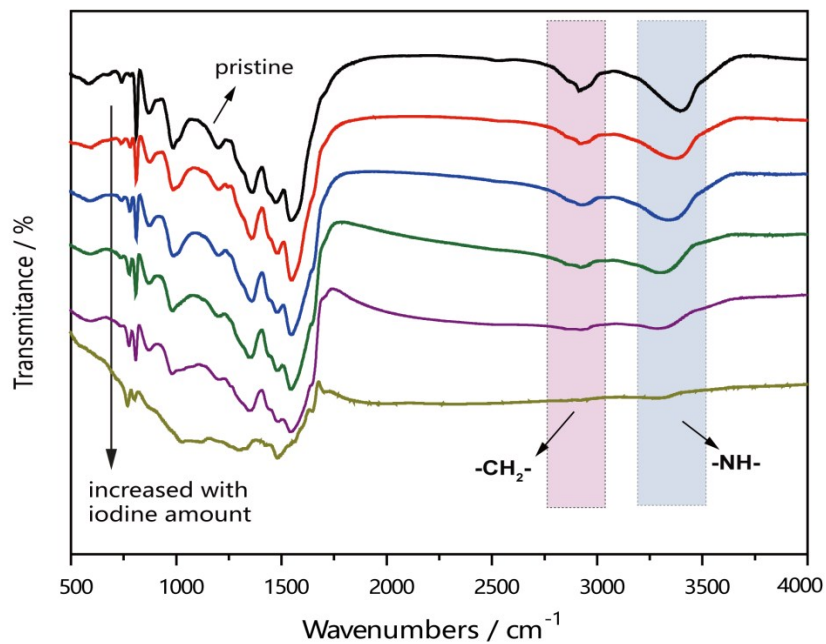


**Figure S12.** FTIR spectra of pristine MFP and I<sub>2</sub>-laden MFPs with different iodine loading weights. The peaks located at ~3400 cm<sup>-1</sup> were associated with NH stretching, and the IR peaks has a significant blue shift (3415.7- 3402.2- 3376.2- 3345.6- 3327.0- 3319.3 cm<sup>-1</sup>) with increasing iodine amount.

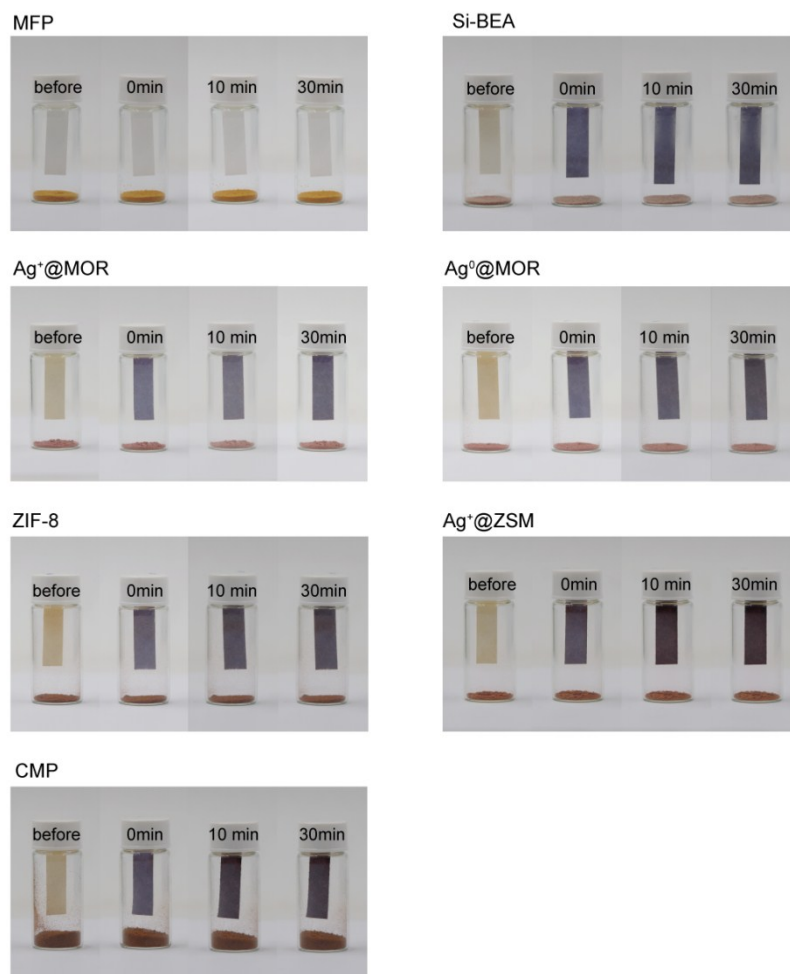


**Figure S13.** Various I<sub>2</sub>-laden adsorption materials were tested for the iodine leaching durability. The photographs were recorded by strips of starch tested papers hung over I<sub>2</sub>-laden samples in a sealed chamber at 298K (before being wetted and 1 second, 10 minute and 0.5 hours after testing).

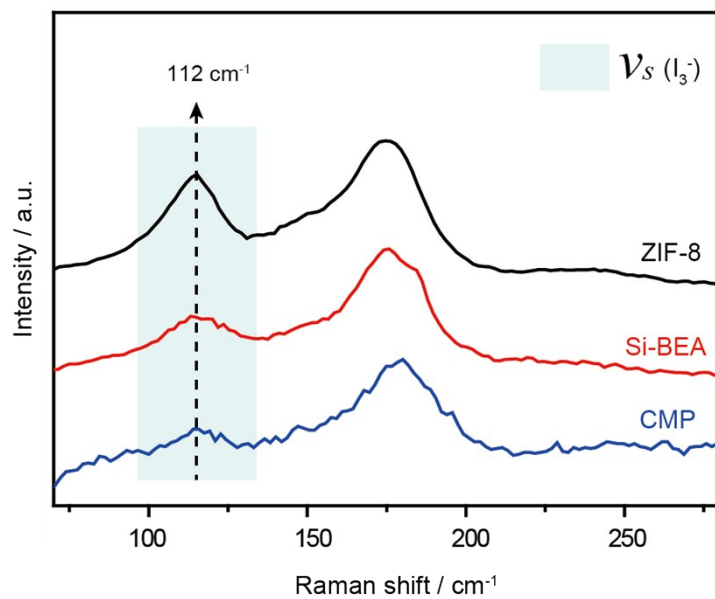


**Figure S14.** Raman spectra of I<sub>2</sub>-laden ZIF-8, Si-BEA, and CMP<sup>4</sup>. All spectra showed significant characteristic peaks of I<sub>3</sub><sup>-</sup> (~112cm<sup>-1</sup>).

CMP\* bound with  $I_3^-$

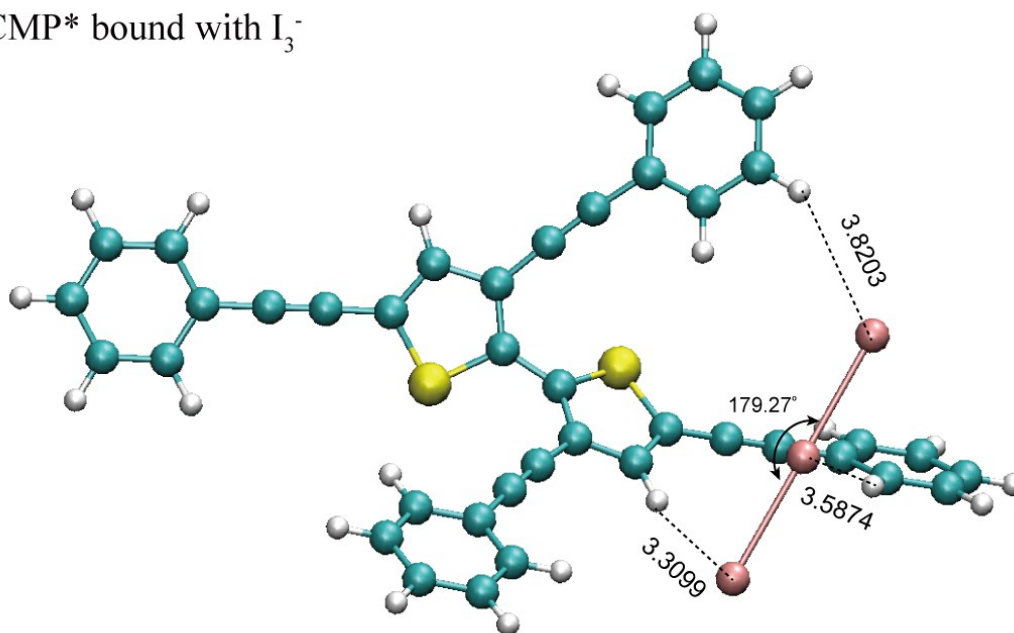


**Figure S15.** The binding energy of  $I_3^-$  and CMP was calculated to be 0.68 kcal/mol.

\*CMP structure from reference 4.

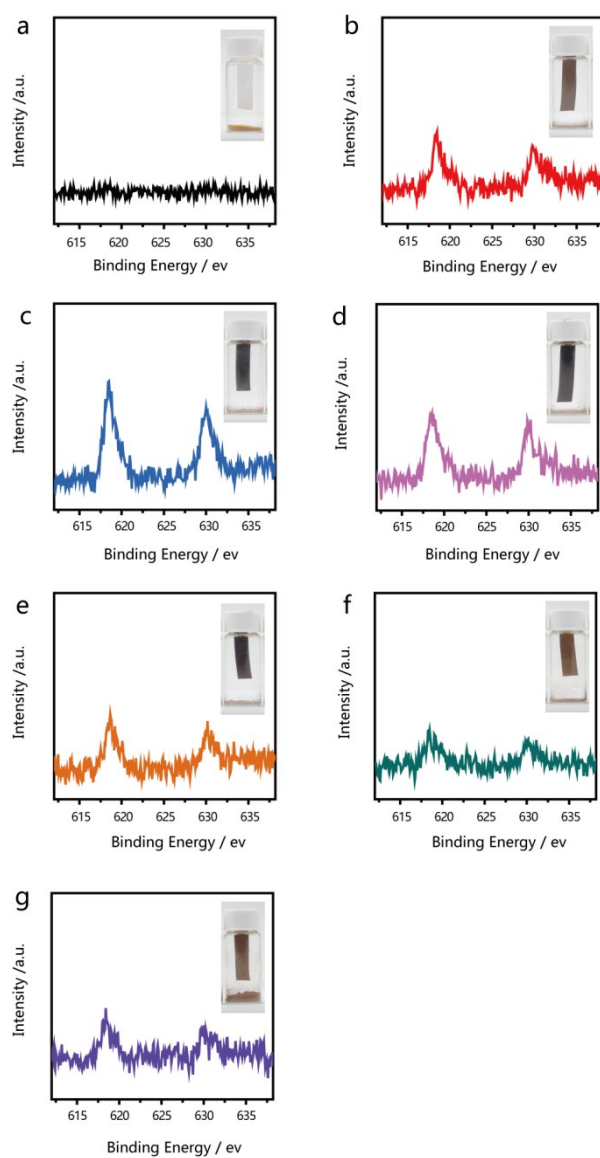


**Figure S16.** Photographs at 6 months after the iodine leaching durability test. The I<sub>2</sub>-laden adsorption materials: **a.** MFP, **b.** Si-BEA, **c.** Ag<sup>+</sup>@MOR, **d.** Ag<sup>0</sup>@MOR, **e.** Ag<sup>+</sup>@ZSM, **f.** ZIF-8 and **g.** CMP.

**Table S5.** The elemental analysis of MFP before and after the I<sub>2</sub> capture and after washing to remove any I<sub>2</sub> from the polymer.

Entry	N /[%]	C /[%]	H /[%]	S /[%]	O /[%]	I /[%]
<b>1</b>	43.76	39.94	5.17	6.38	4.75	0
<b>2</b>	43.85	39.68	5.29	5.85	5.33	0
<b>3</b>	29.4	26.35	3.43	4.16	3.13	33.53
<b>4</b>	29.26	26.42	3.41	4.21	3.21	33.49
<b>5</b>	6.05	5.45	0.72	0.8	0.66	86.32

Renewable test: 1.pristine MFP; 2. I<sub>2</sub>-laden MFP washed by ethanolamine. Iodine in MFP would be thoroughly cleaned out; suggesting MFP could be regenerated via washed using ethanolamine. Leaching durability test: 3. I<sub>2</sub>-laden MFP and 4. I<sub>2</sub>-laden MFP after 6 month. The elemental analysis of two sample indicated that iodine within MFP was very stable and could be maintained even for over 6 months. Maximum capacity: 5. MFP with maximum iodine loading. The corresponding amount of adsorption is 6.31g/g.

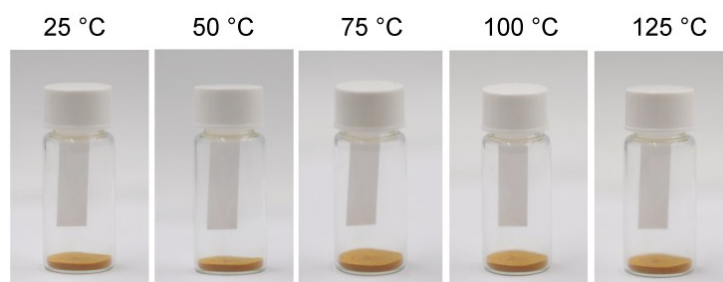


**Figure S17.** The iodine leaching durability test of MFP at different temperatures (298K, 323K, 348K, 373K, 398K, respectively).

**Table S6: The comparisons of the iodine removal performance and synthetic methods of various reported adsorbents.**

Adsorbents	Iodine capacity (mg/g)	Temperature and pressure	$S_{\text{BET}}$ ( $\text{m}^2\text{g}^{-1}$ )	Reusability	Synthetic method	Reference
<b>MFP</b>	6370	398K; 1bar	1440	yes; ethanolamine washing	one-step hydrothermal method	This work
<b>SCIOC-COF-7</b>	4810	348K; 1bar	618	yes; ethanol washing	multistep organic synthesis	7
<b>HCMP-3</b>	3360	358.15 K; 1bar	430	yes; heating	multistep synthesis procedure	8
<b>S<sub>4</sub>-Mg/Al-LDH</b>	1520	350 K	10	yes; ethanol washing	hexamethylenetetramine hydrolysis	9
<b>[Ni<sub>2</sub>(L)(OAc)]ClO<sub>4</sub></b>	2700	294 K; (p(I <sub>2</sub> ) = 29 Pa	< 1.5	-	multistep chemical reactivity	6
<b>PAF-24</b>	2760	298 K; 1bar	136	yes; ethanol washing	modification of porous organic polymers	10
<b>ZIF-8</b>	1250	350 K; 1bar	1875	-	purchased	11
<b>HKUST-1</b>	1750	348 K; 1bar	1798	-	purchased	12
<b>NTP</b>	1800	348 K; 1bar	1067	yes; ethanol washing	cross-coupling reaction	13
<b>NDB-S</b>	4250	348 K; 1bar	116.93	yes; heating	Schiff-base reaction	14
<b>NiP-CMP</b>	2020	350 K; 1bar	2600	yes; ethanol washing	polycondensation reaction	15
<b>AzoPPN</b>	2900	350 K; 1bar	400	yes; ethanol washing	coupling reaction	16
<b>TTPB</b>	3910	350 K;	222	yes; ethanol	Friedel – Crafts	17

		1bar		washing	reaction	
<b>JUC-Z2</b>	5100	333K; 571 Pa	2081	-	multistep chemical reactivity	18
<b>CMPNs</b>	2080	343K; 1bar	1368	-	Cross- coupling reaction	19
<b>SCMP-II</b>	3450	353 K; 1bar	119.76	-	cross- coupling reaction	4

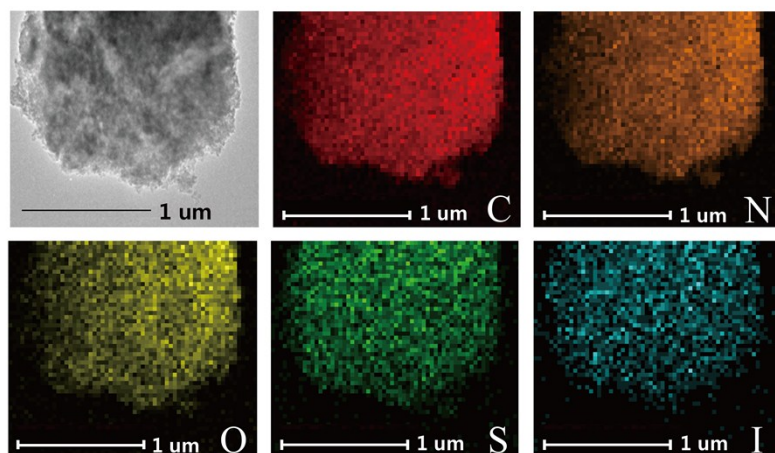


**Figure S18.** Characterization of I<sub>2</sub>-laden MFP: HAADF-STEM image and corresponding elemental mapping images.

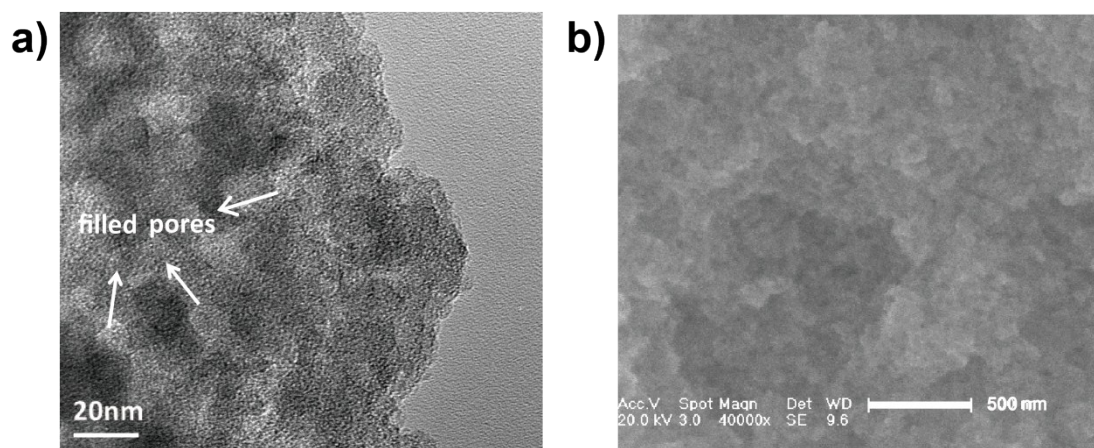


**Figure S19.** The HRTEM image (a) and SEM image (b) of the I<sub>2</sub>-laden MFP.

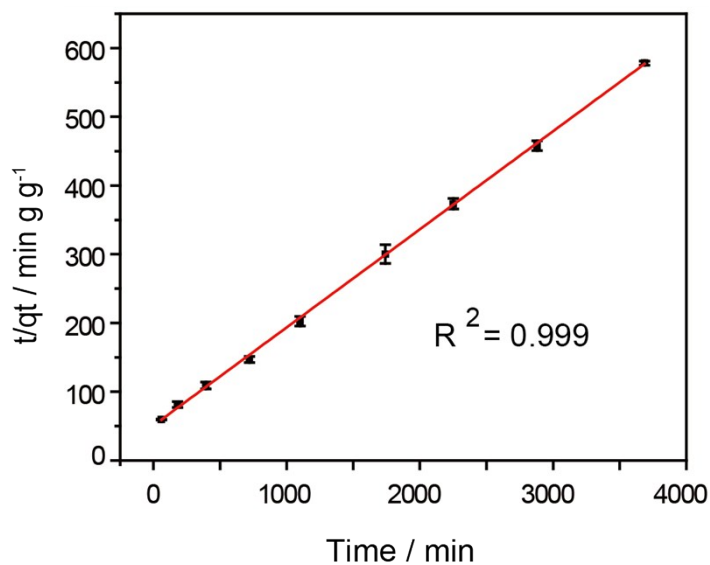


**Figure S20.** The pseudo-second-order kinetic plot for MFP adsorption of iodine. The pseudo-second-order kinetic model has been widely used to describe the characterization of solid adsorbents, which is represented in the form:

$$\frac{t}{q_t} = \frac{1}{k_2 q_e^2} + \frac{t}{q_e}$$

where  $k_2$  ( $\text{g g}^{-1} \text{min}^{-1}$ ) is the rate constant of the pseudo-second-order adsorption,  $q_t$  ( $\text{g g}^{-1}$ ) is the adsorbed amount of iodine at time  $t$  (min), and ( $q_e$ ,  $\text{g g}^{-1}$ ) is the adsorbed amount at equilibrium. The kinetics data were consistent with the pseudo-second-order kinetic model with correlation coefficient  $R^2$  values of 0.999.

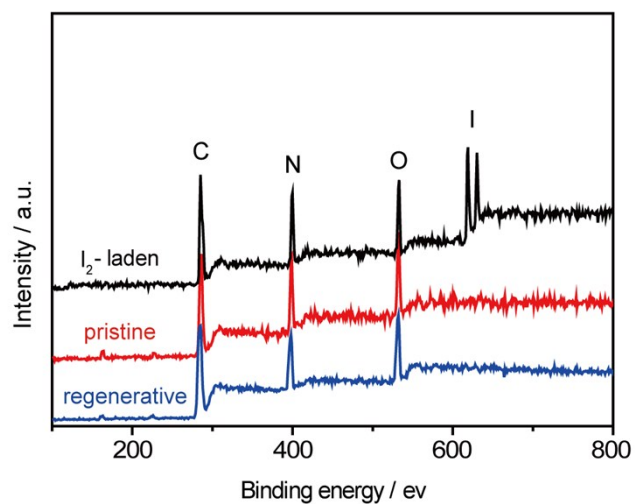


**Figure S21.** XPS spectra of I<sub>2</sub>-laden MFP, pristine MFP, and regenerative MFP. These spectra indicated that iodine species could dissociate thoroughly from MFP upon washed with ethanolamine.

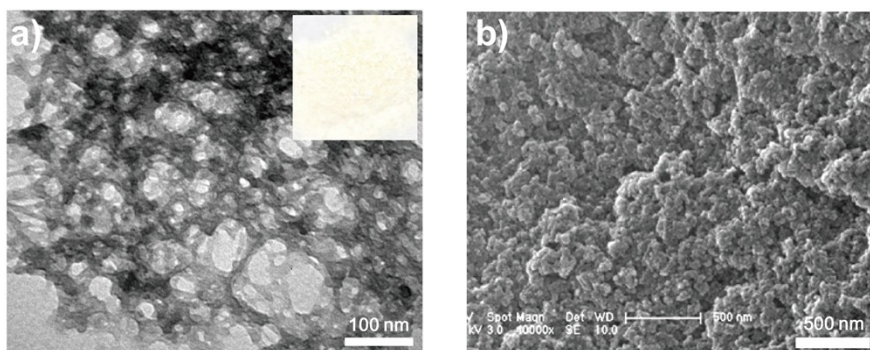


**Figure S22.** Characterization of regenerative MFP: (a) TEM image (insert: photo of regenerative MFP); (b) SEM image indicated no obvious deformation of the polymer after washing by ethanolamine.

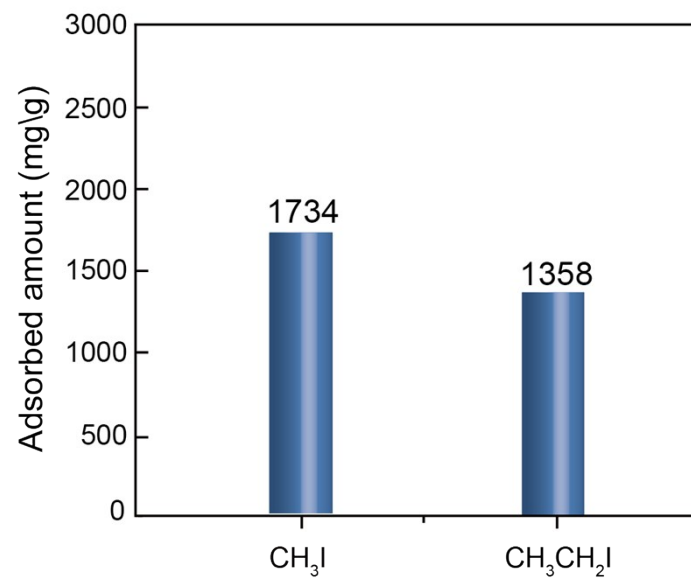


**Figure S23.** The adsorption capacity of MFP on CH<sub>3</sub>I and CH<sub>3</sub>CH<sub>2</sub>I.

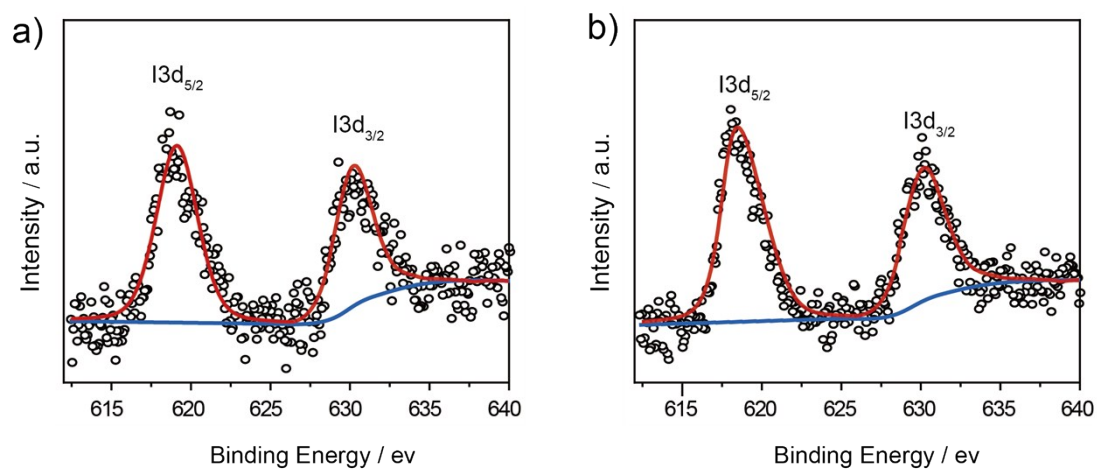


**Figure S24.** XPS spectra of  $\text{CH}_3\text{I}$ -laden MFP and  $\text{CH}_3\text{CH}_2\text{I}$ -laden MFP.

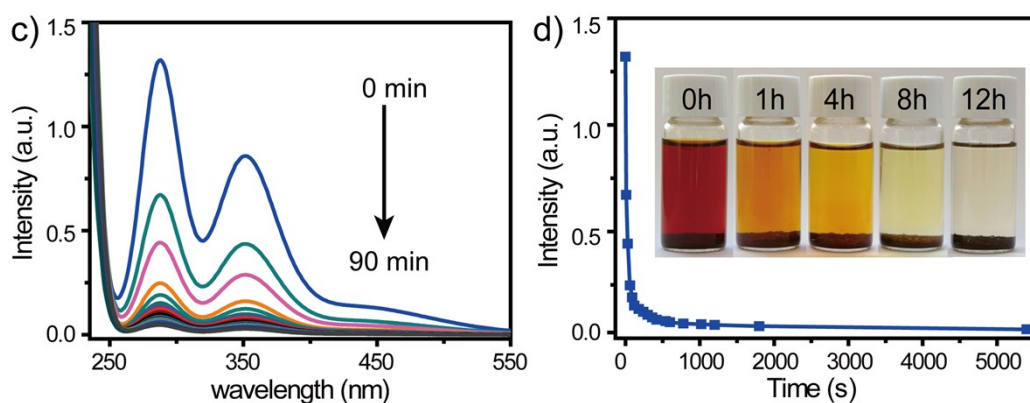


**Figure S25.** The capture of  $I_2$  from water were performed at room temperature under continuous stirring were evaluated by UV/vis spectroscopy. For accurate values, the solutions are diluted in equal proportion before performed UV-Vis absorption analysis. (a) The temporal evolution UV/vis spectra for the absorption of  $I_2$  in aqueous solution (1% Lugol ( $I_2$ -KI) solution<sup>20</sup>) over 90 min. (b) Kinetics curve of MFP versus contact time in aqueous solution (insert: color change at different time intervals). The colors of the solutions faded slowly and finally to colorless, which indicated that the iodine was encapsulated into the MFP networks to successively generate  $I_2$ -laden systems.

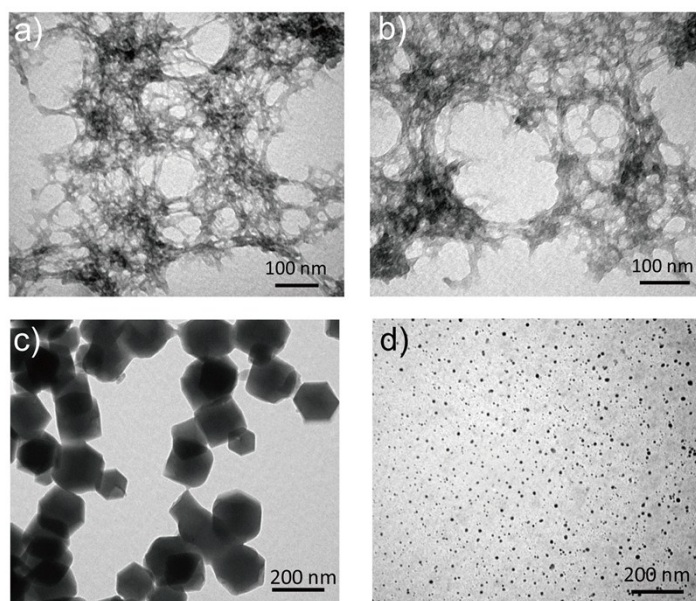


**Figure S26.** TEM images of MFP and ZIF-8 before and after immersed in 5M  $\text{HNO}_3$ : (a) MFP before immersed; (b) MFP after immersed; (c) ZIF-8 before immersed; (d) ZIF-8 after immersed.

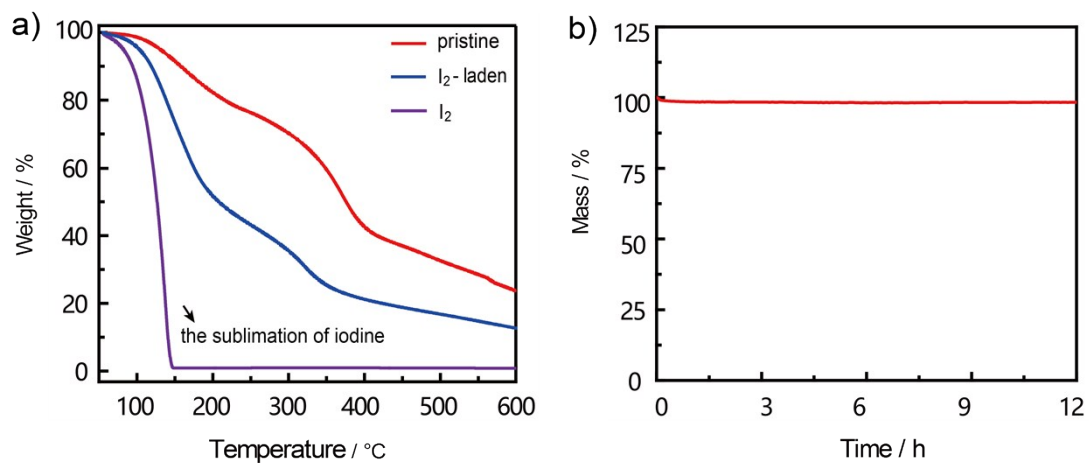


**Figure S27.** The thermal stability of MFP was also examined. (a) The TG profiles of pristine MFP, I<sub>2</sub>-laden MFP, and I<sub>2</sub>. (b) The isothermal TG profile of pristine MFP at 125 °C for 12 h. This showed that MFP remained stable and did not lose mass after being heated to 125 °C and standing for 12 h. The excellent thermal stability of MFP enabled its utilization at high operating temperatures required for nuclear waste disposal.

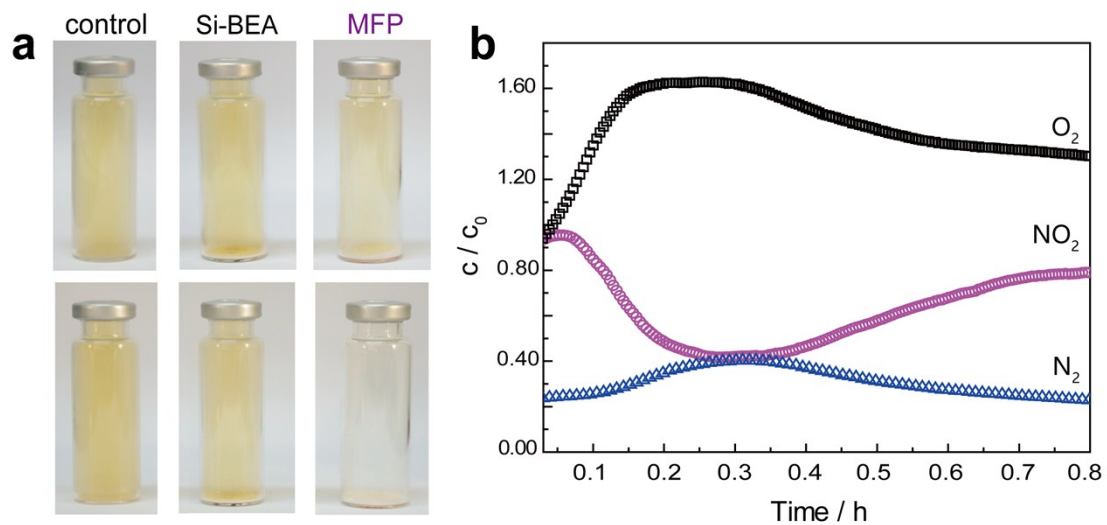


**Figure S28.** (a) Photographs show the NO<sub>2</sub> adsorption behaviors of control sample, Si-BAE and MFP when immersed in 20,000 ppm NO<sub>2</sub> at initial and 5 min intervals; (b) The NO<sub>2</sub> microbreakthrough curve for activated MFP. The capacity was calculated to be 13.88 ml NO<sub>2</sub> per g MFP.

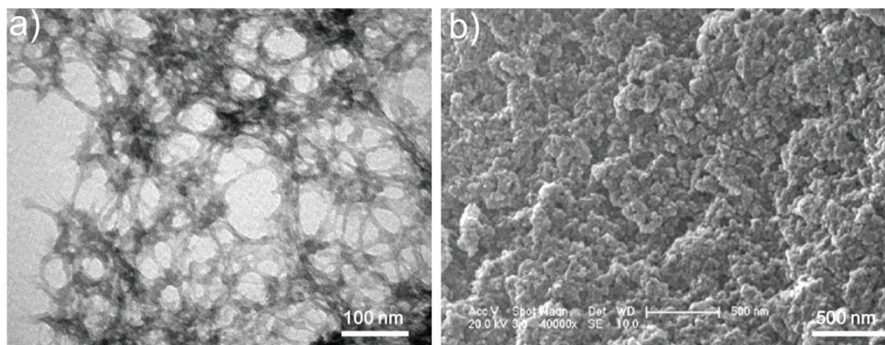


**Figure S29.** Characterization of MFP after NO<sub>2</sub> absorption: (a) TEM image; (b) SEM image.

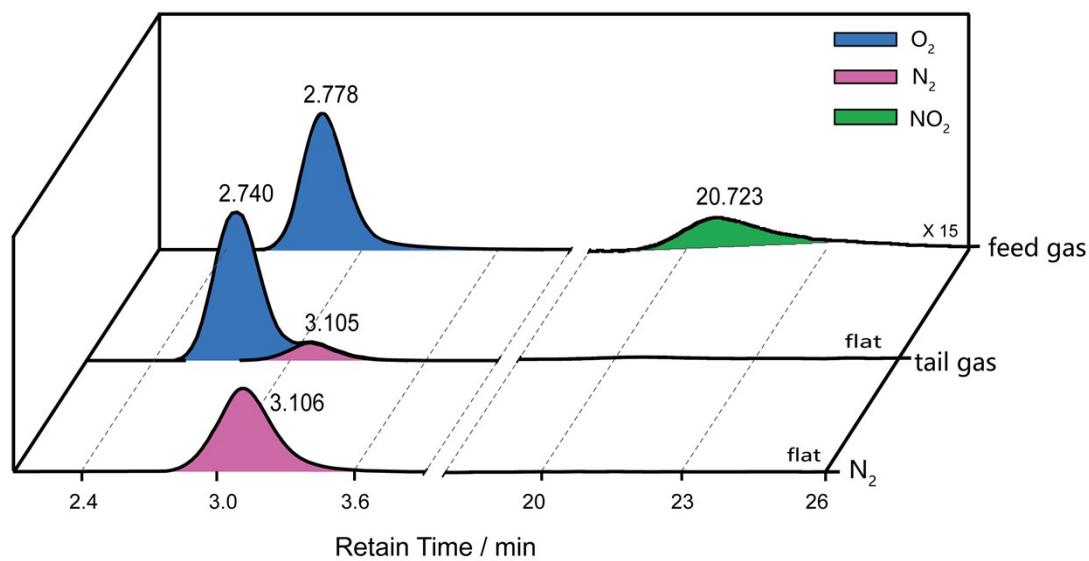


**Figure S30.** The behavior of removing nitrogen dioxide by MFP. Gas chromatograph of feed gas: ternary gas mixtures (O<sub>2</sub>: 10% / NO<sub>2</sub>: 20% / Ar: 70%); tail-gas: mixed gas pass through MFP adsorbent and pure nitrogen as a standard gas. The argon used as sweep gas.

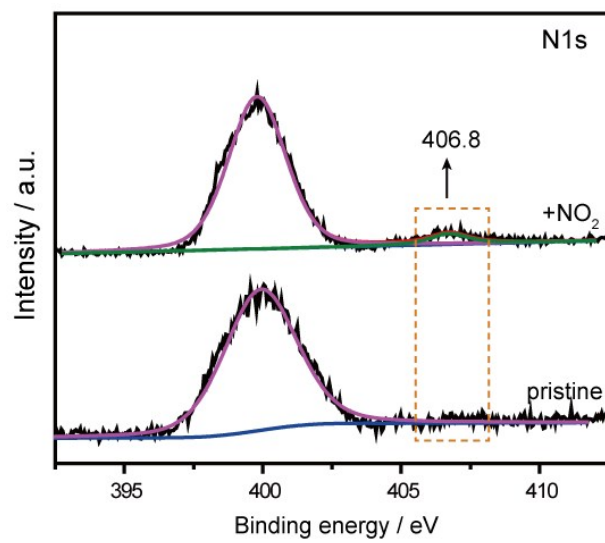


**Figure S31.** Nitrogen 1s XPS data for pristine MFP and NO<sub>2</sub> exposed sample.

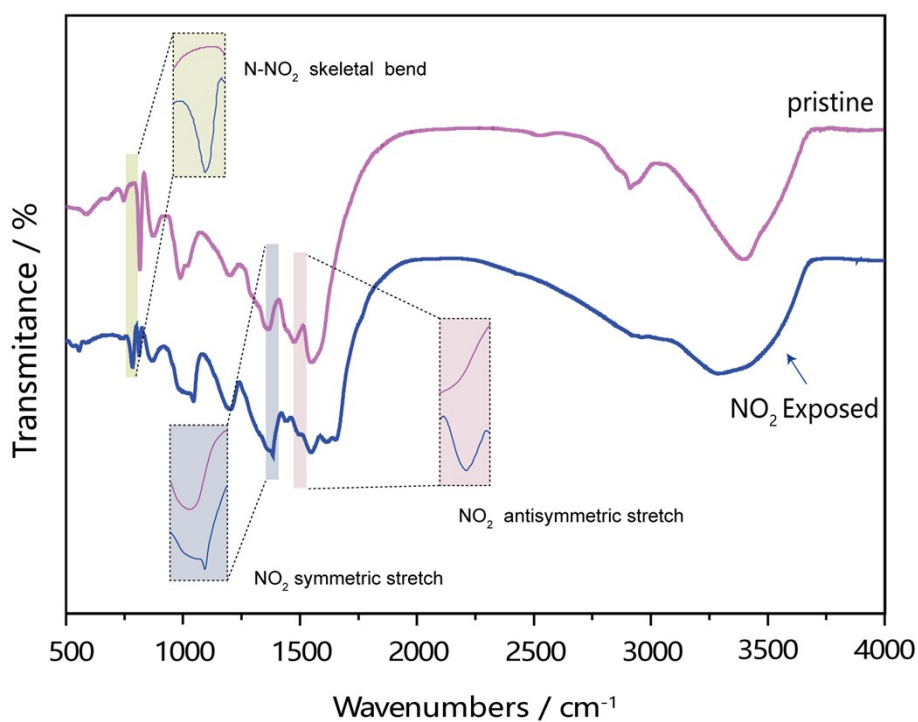


**Figure S32.** FTIR shown that a new band appearing at 780 cm<sup>-1</sup> corresponding to the N-NO<sub>2</sub> skeletal bend group and the vibrations from nitro groups of nitramines (N-NO<sub>2</sub>) are seen at 1500 cm<sup>-1</sup> (NO<sub>2</sub> antisymmetric) and 1350 cm<sup>-1</sup> (NO<sub>2</sub> symmetric).

## References

- 1 T. C. T. Pham, S. Docao, I. C. Hwang, M. K. Song, D. Y. Choi, D. Moon, P. Oleynikov and K. B. Yoon, *Energy Environ. Sci.*, 2016, **9**, 1050-1062.
- 2 S. Aguado, G. Bergeret, C. Daniel and D. Farrusseng, *J. Am. Chem. Soc.*, 2012, **134**, 14635-14637.
- 3 G. Lu, S. Li, Z. Guo, O. K. Farha, B. G. Hauser, X. Qi, Y. Wang, X. Wang, S. Han, X. Liu, J. S. DuChene, H. Zhang, Q. Zhang, X. Chen, J. Ma, S. C. Loo, W. D. Wei, Y. Yang, J. T. Hupp and F. Huo, *Nat. Chem.*, 2012, **4**, 310-316.
- 4 F. Ren, Z. Zhu, X. Qian, W. Liang, P. Mu, H. Sun, J. Liu and A. Li, *Chem. Commun.*, 2016, **52**, 9797-9800.
- 5 R. A. Molla, M. A. Iqbal, K. Ghosh, Kamaluddin and S. M. Islam, *Dalton Trans.*, 2015, **44**, 6546-6559.
- 6 M. Golecki, N. Beyer, G. Steinfeld, V. Lozan, S. Voitekhovich, M. Sehabi, J. Mollmer, H. J. Kruger and B. Kersting, *Angew. Chem. Int. Ed.*, 2014, **53**, 9949-9952.
- 7 Z. J. Yin, S. Q. Xu, T. G. Zhan, Q. Y. Qi, Z. Q. Wu and X. Zhao, *Chem. Commun.*, 2017, **53**, 7266-7269.
- 8 Y. Z. Liao, J. Weber, B. M. Mills, Z. H. Ren and C. F. J. Faul, *Macromolecules*, 2016, **49**, 6322-6333.
- 9 S. L. Ma, S. M. Islam, Y. Shim, Q. Y. Gu, P. L. Wang, H. Li, G. B. Sun, X. J. Yang and M. G. Kanatzidis, *Chem. Mater.*, 2014, **26**, 7114-7123.
- 10 Z. Yan, Y. Yuan, Y. Tian, D. Zhang and G. Zhu, *Angew. Chem. Int. Ed.*, 2015, **54**, 12733-12737.
- 11 J. T. Hughes, D. F. Sava, T. M. Nenoff and A. Navrotsky, *J. Am. Chem. Soc.*, 2013, **135**, 16256-16259.
- 12 D. F. Sava, K. W. Chapman, M. A. Rodriguez, J. A. Greathouse, P. S. Crozier, H. Zhao, P. J. Chupas and T. M. Nenoff, *Chem. Mater.*, 2013, **25**, 2591-2596.
- 13 H. Ma, J. J. Chen, L. X. Tan, J. H. Bu, Y. H. Zhu, B. Tan and C. Zhang, *Acs. Macro. Letters.*, 2016, **5**, 1039-1043.
- 14 Z. Guo, P. Sun, X. Zhang, J. Lin, T. Shi, S. Liu, A. Sun and Z. Li, *Chem. Asian. J.*, 2018.
- 15 A. Sigen, Y. Zhang, Z. Li, H. Xia, M. Xue, X. Liu and Y. Mu, *Chem. Commun.*, 2014, **50**, 8495-8498.
- 16 H. Li, X. Ding and B. H. Han, *Chemistry*, 2016, **22**, 11863-11868.
- 17 T. Geng, Z. Zhu, W. Zhang and Y. Wang, *J. Mater. Chem. A*, 2017, **5**, 7612-7617.
- 18 C. Pei, T. Ben, S. Xu and S. Qiu, *J. Mater. Chem. A*, 2014, **2**, 7179-7187.
- 19 Y. F. Chen, H. X. Sun, R. X. Yang, T. T. Wang, C. J. Pei, Z. T. Xiang, Z. Q. Zhu, W. D. Liang, A. Li and W. Q. Deng, *J. Mater. Chem. A*, 2015, **3**, 87-91.
- 20 J. He, J. Duan, H. Shi, J. Huang, J. Huang, L. Yu, M. Zeller, A. D. Hunter and Z. Xu, *Inorg. Chem.*, 2014, **53**, 6837-6843.